ELSEVIER

Journal of Molecular Catalysis A: Chemical 107 (1996) 55–65

JOURNAL OF MOLECULAR CATALYSIS A: CHEMICAL

PTRF X-ray absorption fine structure as a new technique for catalyst characterization

W.-J. Chun, M. Shirai, K. Tomishige, K. Asakura, Y. Iwasawa *

Department of Chemistry, Graduate School of Science, The University of Tokyo, Hongo, Bunkyo-ku, Tokyo 113, Japan

Abstract

A chamber for observation in situ of polarized total-reflection fluorescence extended X-ray absorption fine structure (PTRF-XAFS) spectra was constructed, which makes it possible to measure the PTRF-XAFS spectra in situ under preparation, treatment, and reaction conditions from high vacuum(1×10^{-9} Pa) to high pressure(1×10^{5} Pa) and from low temperature(100 K) to high temperature(800 K). The PTRF-XAFS technique can provide information on asymmetric or anisotropic structure of active metal and metal–oxide sites supported on single crystal substrates as models for supported catalysts, by measuring bondings of supported species in two or three different directions parallel and perpendicular to the surface independently. Typical EXAFS and XANES spectra for Cu^{2+}/α-SiO_2 (0001), CoO_x/α-Al_2O_3 (0001), $[Pt]_4/\alpha$-Al_2O_3 (0001), and V_2O_5/ZrO_2 (100) taken by the PTRF-XAFS chamber are discussed in relation to their catalytic properties.

Keywords: X-ray absorption fine structure (XAFS); Chamber in situ XAFS; Asymmetric structure analysis; Anisotropic structure analysis; Orientation of surface bonds; Surfaces

1. Introduction

Structures of metal and metal–oxide sites at support surfaces which show catalytic performance may be asymmetric or anisotropic, reflecting asymmetric or anisotropic structures of support surfaces and asymmetric or anisotropic interaction mode at the interface between metal or metal oxide and support. Their structures may also change asymmetrically or anisotropically during treatment of catalysts under vacuum, H_2, or O_2, or under catalytic reaction conditions. In order to explore the relation between surface structure and catalytic property and to clarify the genesis of solid catalysis and also to understand catalytic reaction mechanisms, detailed information is needed on the structure and dynamic change of active sites in two–three different directions. This sort of molecular-level information may provide a way to improve conventional catalysis to more efficient performance and also a way to develop new selective catalytic systems [1–3].

EXAFS (extended X-ray absorption fine structure) and XANES (X-ray absorption near-edge structure) have been well recognized to be a powerful technique to characterize catalytic materials [4,5]. In the case of powder samples such as typical heterogeneous catalysts, the structures determined by the above XAFS (X-ray absorption fine structure) technique in a traditional transmission mode are averaged structures in every direction of a sample, which prevents the structures at catalyst

* Corresponding author. Fax: (+81-3)58006892, e-mail: iwasawa@chem.s.u-tokyo.ac.jp

SSDI 1381-1169(95)00163-8

surfaces being precisely characterized. When flat substrates such as single crystals, polished glasses and amorphous substrates, and so on, are employed as supports, however, characterization of metal and metal–oxide sites on them can be achieved separately in two different bond directions parallel and normal to the surface by polarized X-rays stemming from synchrotron radiation.

EXAFS oscillation $\chi(k)$ is given by Eq. (1) based on a single scattering theory [6,7].

$$\chi(k) = \Sigma N_i^* A_i^*(k) \sin(2kR_i + \phi_i(k)) \quad (1)$$

$$A_i^*(k) = F_i(k) \exp(-2\sigma_i^2 k^2) \exp(-2R_i/\lambda_i(k))/kR_i^2 \quad (2)$$

where N_i^*, R_i and $\sigma_i(k)$ represent effective coordination number of the ith shell, interatomic distance and phase shift function. $F_i(k)$, ϕ_i and λ_i stand for amplitude function, Debye–Waller factor and mean free path of photoelectron. Effective coordination number (N_i^*) of K-edge XAFS spectra has a cosine square dependence on the angle (θ_j) between polarization direction of the electric-field vector of the incident X-ray and direction of bonding or direction of the unoccupied bound state orbital (Eq. (3)) [8]. In the case of LIII-edge spectra, N_i^* is expressed by Eq. (4) [8].

For K-edge spectra,

$$N_i^* = 3\Sigma\cos^2\theta_j \quad (3)$$

For LIII-edge spectra,

$$N_i^* = 0.7N_i + 0.9\Sigma\cos^2\theta_j \quad (4)$$

Thus, when the polarization of the incident X-ray is normal to the surface (p-polarization), the X-ray absorber's neighbors which lie along lines parallel to the surface do not contribute to XAFS signals. These bonds are observable when s-polarized X-rays parallel to the surface are used. Conversely, the bonds normal to the surface are detectable by p-polarized XAFS.

The problem in applying conventional XAFS spectroscopy performed in a transmission mode to single crystal or flat amorphous samples is a low concentration of surface species. Although a fluorescent detection method of XAFS spectra can be used for dilute samples, the strong elastic scattering from the bulk hinders detection of the fluorescence from the surface metal sites in a hard X-ray region. one way to enhance the signal to background ratio (S/B) is to use the total-reflection method. When X-rays strike the sample with a glancing angle less than the critical angle, total-reflection of the incident X-ray occurs where the penetration depth of X-ray into the bulk is less than 3 nm and the elastic scattering X-ray from the bulk is remarkably reduced [9–12]. Thus, total-reflection fluorescence XAFS technique can be applied to surface species below monolayer [13,14].

In the present paper we report development of an instrument which makes it possible to carry out preparation in situ of samples and measurement in situ of polarized total-reflection fluorescence XAFS (PTRF-XAFS) under reaction conditions. In addition to the adjustment of total-reflection conditions, the sample orientation relative to the polarized X-ray can be variable in the PTRF-XAFS chamber without exposure to air. By using the PTRF-XAFS apparatus, we also report the characterization of metal and metal–oxide sites supported on single crystals in Cu^{2+}/α-SiO_2 (0001) [15], CoO_x/α-Al_2O_3 (0001) [16–19], $[Pt]_4/\alpha$-Al_2O_3 (0001) [17], and V_2O_5/ZrO_2 (100) [20].

2. In situ PTRF-XAFS chamber

Design of the apparatus is illustrated in Fig. 1 [17,21]. Metallic and metal–oxide species are deposited on a flat substrate by metal evaporation or chemical vapor deposition (CVD) of metal–organic precursors. In order to prevent the deposition of the evaporated metals or metal organics on the Be windows, the chamber is separated into two parts by a gate valve. The sample is prepared in the upper part where an evaporation source and a quartz crystal thickness monitor are present. When XAFS spectra are measured, the sample is moved down to the lower part by a long flexible

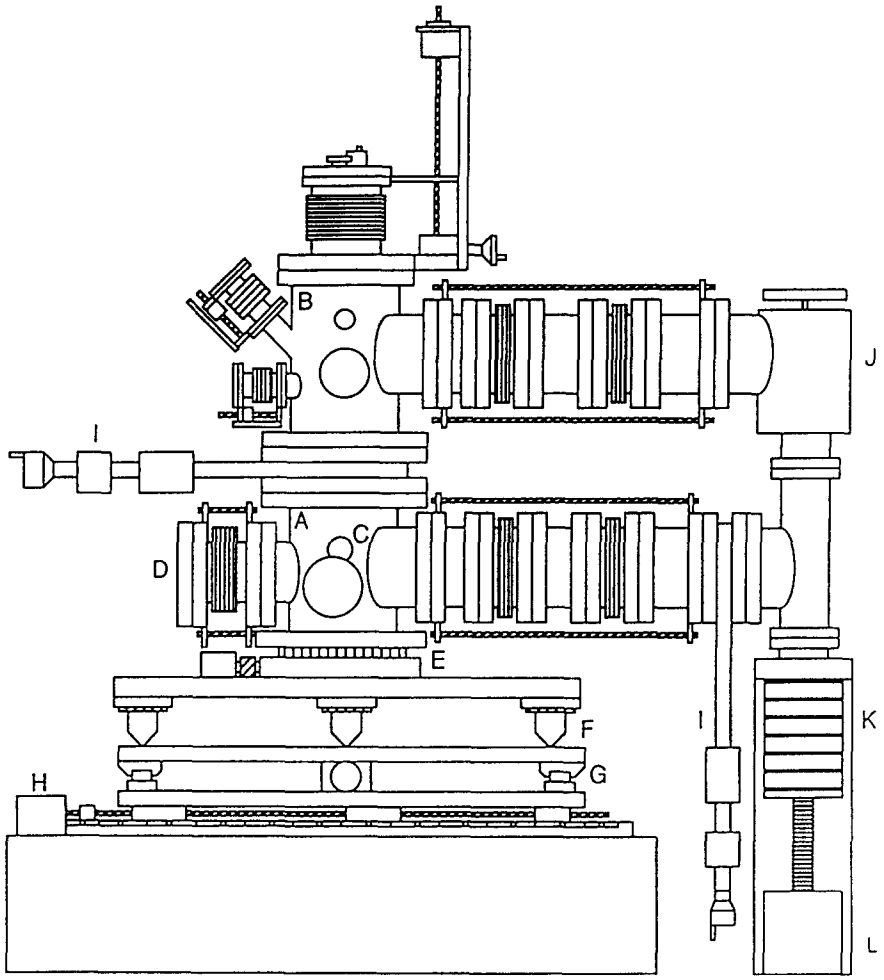

Fig. 1. In situ polarized total-reflection fluorescence XAFS equipment; A: measurement chamber; B: preparation chamber; C: window for reflected X-ray beam; D: window for fluorescence X-ray; E: rotation table; F: Z-table; G: X-table; H: Y-table; I: gate valve; J: angle valve; K: diffusion pump: L: rotary pump.

bellow attached to the top of the preparation chamber.

The lower part has three Be windows (thickness: 25 μm, purity: 99.8%, Electrofusion Corporation) for incident, reflected, and fluorescent X-rays. Be foils are fixed at the ports with a structure adhesive material. The diameter of the Be windows for the fluorescent X-ray is 50 mm in diameter and it is possible to bring the Be window close to the sample with a linear motion drive. Thus, we can detect 50% of 4π sr of total-fluorescence X-ray when the sample surface is set parallel to the fluorescence window. Reaction gases can be introduced into the chamber through a leak valve.

We adopted the *XYZ* and rotary tables on which the whole chamber is mounted to adjust total-reflection conditions. The *XYZ* and rotary tables are driven by stepping motors controlled with a personal computer. The *XYZ* and rotary tables are composed of four parts. The top is a rotation table which can rotate with a precision of 0.02 mrad. The second one is a *Z*-table composed of three vertical jacks which are positioned in an equilateral triangle; one in the front and the other two at the back in Fig. 1. The sample center is put over the mass center of this triangle. The two bottom tables are *X*- and *Y*-tables. Total-reflection conditions for s-polarization with respect to the surface (E//surface) are adjusted by use of the three ver-

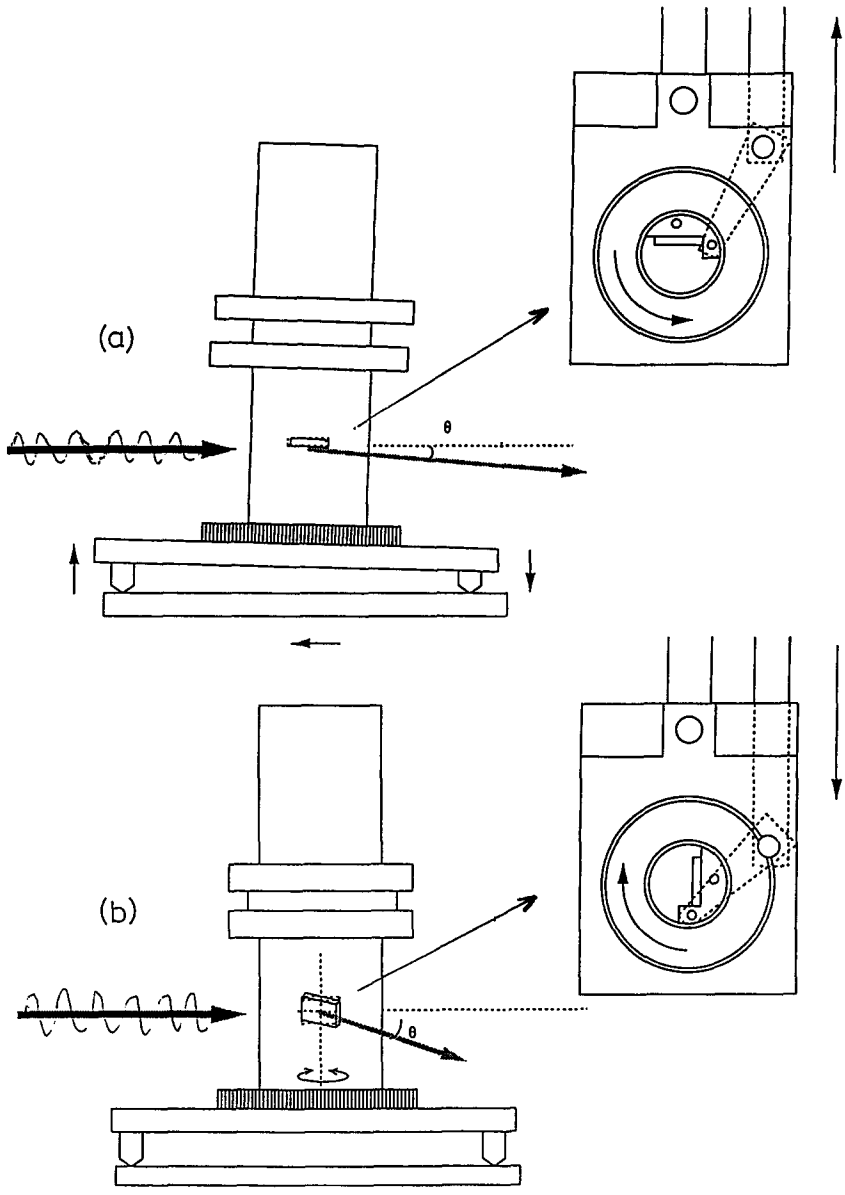

Fig. 2. Adjustment for (a) p-polarized and (b) s-polarized orientations by a rotation mechanism.

tical jacks and the *X*-table, respectively, as shown in Fig. 2 [21]. When the sample is tilted by the three vertical jacks, the *X*-table is moved by a calculated amount to set the X-ray beam to irradiate the same position of the sample. The angle resolution for p-polarization is 0.02 mrad and that for s-polarization is also 0.02 mrad. The sample holder is fixed to a cylinder which is connected to two bearing rotors. The cylinder can be rotated by 100 deg and the sample orientation relative to the polarized X-ray can be altered from the parallel arrangement to the perpendicular one [21].

The sample can be heated up to 873 K from backside using a Ta resistive heating sheet. An α-Al_2O_3 sheet ($70\times16\times0.5$ mm^3 or $70\times16\times1$ mm^3, purity: 99.8%, Degussa, Japan) is mounted between the sample and the Ta sheet which has a large thermal conductivity and at the same time is a good electric insulator. The temperature of the sample is measured by a thermocouple fixed to

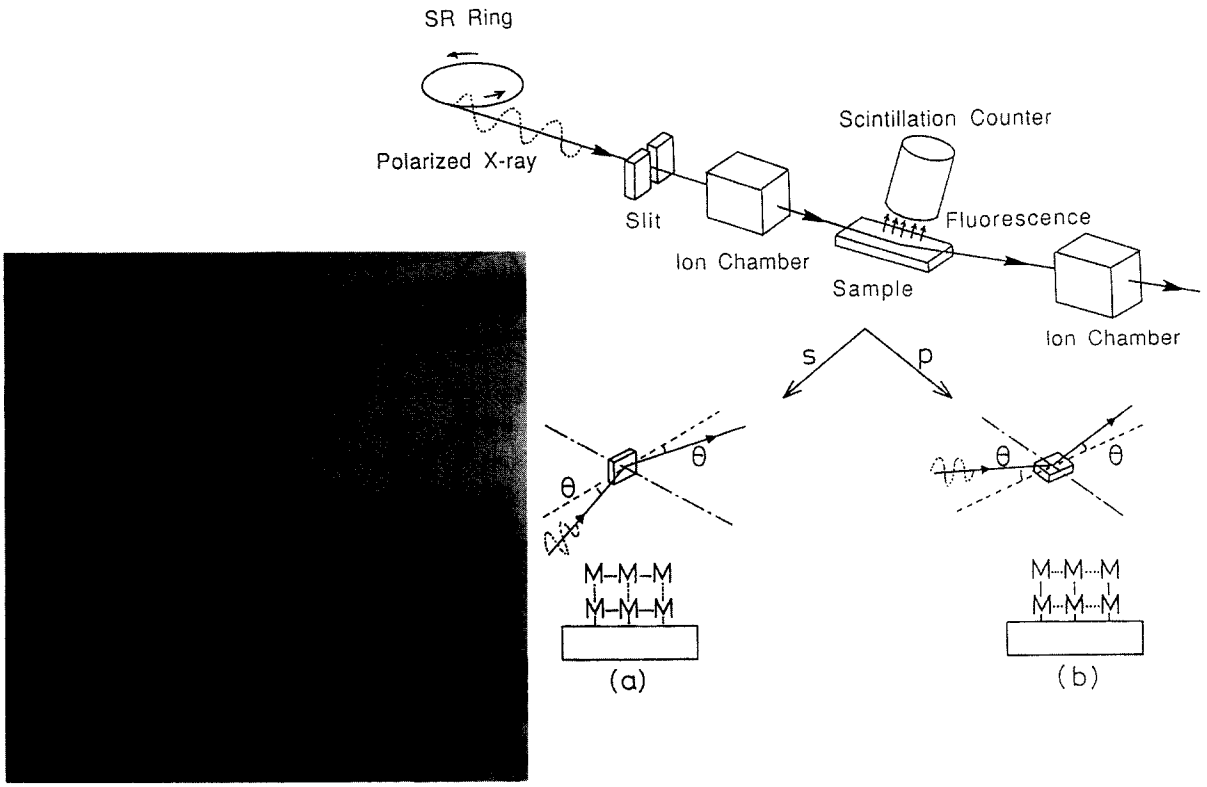

Fig. 3. Schematic diagram of polarized total-reflection fluorescence XAFS and a photograph of the apparatus.

the sample by a glue for a high temperature use. The sample can also be cooled to 100 K by liquid N_2 which is flowed through a tube attached to the sample holder. The cooling of the sample is due to reduction of the Debye–Waller factor of EXAFS oscillation, if necessary.

The PTRF-XAFS apparatus is illustrated in Fig. 3, where a photograph of the equipment is also shown. By using the PTRF-XAFS equipment, one can perform measurement in situ of the structures of metallic and metal–oxide sites supported on flat inorganic support surfaces (single crystals or amorphous substrates) under a variety of treatment and reaction conditions.

3. PTRF-XAFS measurements

Pt LIII-edge, V K-edge, Co K-edge and Cu K-edge XAFS spectra for the samples described below were measured at BL-7C, BL-7C, BL-14A, and BL-14A stations, respectively, of the Photon Factory using a sagittal focussing Si (111) double crystal monochromator in the National Laboratory for High Energy Physics (KEK-PF) as shown in Fig. 3 (Proposal No. 92-032, 92G-174, 89-146 and 90-142, and 85-011, respectively). Higher harmonics was removed by a total-reflection mirror between the monochromator and the X-ray monitor. The incident and reflected X-ray beams on the sample surface were monitored by N_2-filled ionization chambers. The fluorescent X-ray was detected by a NaI scintillation counter. The X-ray Bragg diffraction peaks form the crystalline substrate could be removed by placing small pieces of Pb sheets, when necessary, in front of the window of a scintillation counter at a position where the Bragg diffraction begins to appear.

4. Results and discussion

The characterization of metallic and metal–oxide sites at model surfaces by the PTRF-XAFS

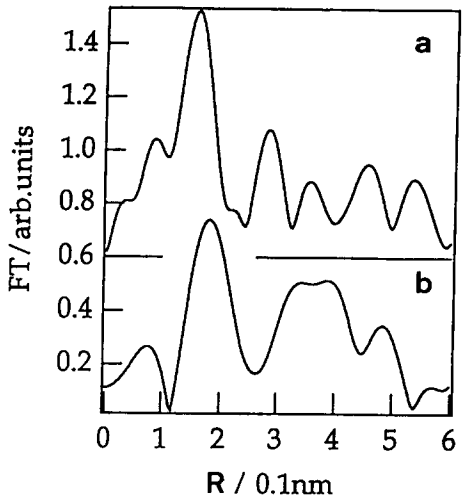

Fig. 4. Fourier transforms of the incipient supported Pt_4/α-Al_2O_3 (0001) in (a) p-polarization and (b) s-polarization.

technique are described in the section. The catalytic performance of the samples is also reported.

4.1. Platinum clusters on α-Al_2O_3 (0001)

Fig. 4 shows the Fourier transforms of k^2-weighted EXAFS oscillations of the supported Pt_4 clusters for s- and p-polarizations over the k region 30–90 nm^{-1} [22]. The supported cluster sample was prepared by a drop-wise impregnation method using CH_2Cl_2 solution of $Pt_4(CH_3COO)_8$ followed by evacuation for desiccation. In contrast to the Fourier transform of the EXAFS data for $Pt_4(CH_3COO)_8$ (Pt–Pt: 0.251 nm, Pt–O: 0.217 nm and 0.201 nm) which shows a Pt–Pt peak around 0.24 nm besides a Pt–O peak around 0.18 nm (phase shift uncorrected), no peak due to Pt–Pt bond was observed with both polarizations in Fig. 4. The EXAFS data clearly demonstrate that Pt–Pt bonding was cleaved upon supporting of the Pt_4 cluster on the alumina [17]. On the other hand, Pt–O bonds were observed in s- and p-polarized EXAFS data and the coordination number of the bonds was determined by a curve fitting method to be 3.5 and 3.2 for s- and p-polarization, respectively. From the model calculation based on the unreconstructed α-Al_2O_3 (0001) surface structure, we can conclude that Pt atoms were located on the three-fold hollow sites composed of the topmost oxygen atoms of the surface.

The sample was reduced with H_2 at 393 K. The observed Pt LIII-edge XAFS spectra in both polarizations are shown in Fig. 5. The Fourier transforms of k^2-weighted EXAFS data are also shown in Fig. 5. A peak around 0.24 nm corresponding to Pt–Pt was observed more strongly in s-polarization than in p-polarization. The Pt–Pt bond distance was determined to be 0.271 nm by the curve fitting analysis. Effective coordination numbers (N^*) were also determined as 6 and 3 for s- and p-polarizations, respectively. Although the absolute value of N^* is hardly obtained because of the narrow k range available, the ratio of the N_p^* to N_s^* in two polarized directions can give more reliable estimation for the orientation of Pt clusters. The ratio N_p^*/N_s^* is nearly 0.5, which suggests that Pt clusters must lie parallel to the α-Al_2O_3 (0001) plane. We calculated the ratios N_p^*/N_s^* assuming several Pt cluster models. If Pt clusters had a double-layer structure parallel to the substrate plane, the ratio would become as large as 0.9. If Pt clusters had a symmetric structure like sphere, the ratio would be 1.0, where there is no difference with s- and p-polarizations. Only one atomic-layer model, which gives the ratio to be 0.6, can explain the experimental value [22]. By subsequent reduction of the sample with H_2 at 673 K, aggre-

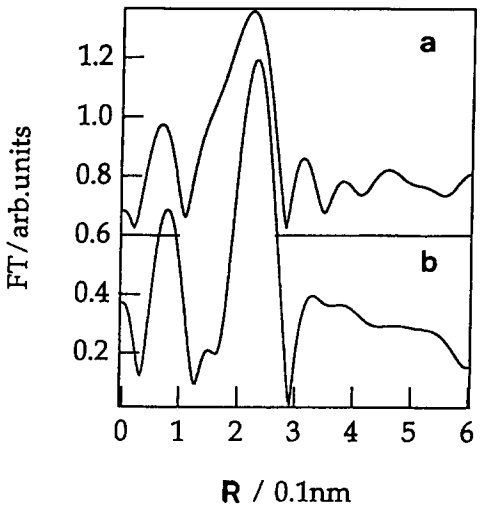

Fig. 5. Fourier transforms of Pt_4/α-Al_2O_3(0001) after reduction with H_2 at 393 K in (a) p-polarization and (b) s-polarization.

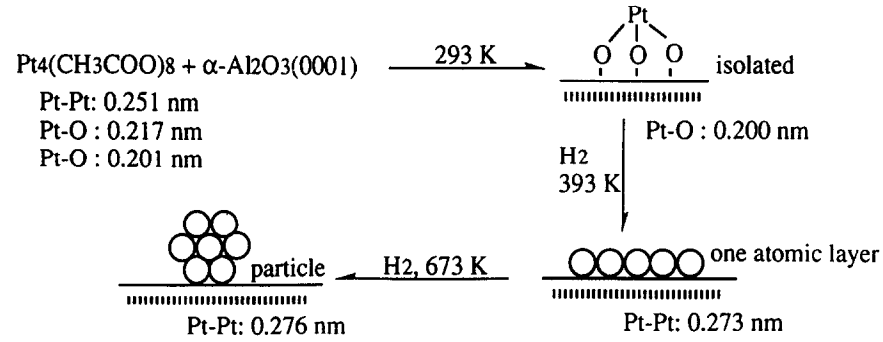

Fig. 6. Structure transformation of the Pt_4 cluster at α-Al_2O_3(0001) surface. The number of Pt atoms in the one atomic layer and the particle does not mean the their sizes.

gation of Pt atoms to three-dimensional particles was observed, showing a typical EXAFS oscillation of metallic Pt–Pt bond for Pt particles. The surface structure transformations are illustrated in Fig. 6.

4.2. Copper oxide on α-quartz (0001)

The samples were prepared as follows [15]. After an α-quartz (0001) substrate was treated at 393 K for 2 h in air, $Cu(DPM)_2$ vapor (DPM: dipyvaloylmethanate) was deposited on the quartz surface for 4 h by CVD at 373 K for the vaporization and at 473 K for the deposition in a flow of dried air (20 cm^3/min). Then the sample was calcined at 673 K for 2 h. The treatment of the sample at 673 K may transform α-quartz (0001) to the β-type at least at the surface layers, which has a more ordered structure. The ratio of Cu atom to surface oxygen atom on the quartz substrate was estimated to be 0.4 by an ICP analysis of the solution sample obtained by leaching the Cu ions at the surface.

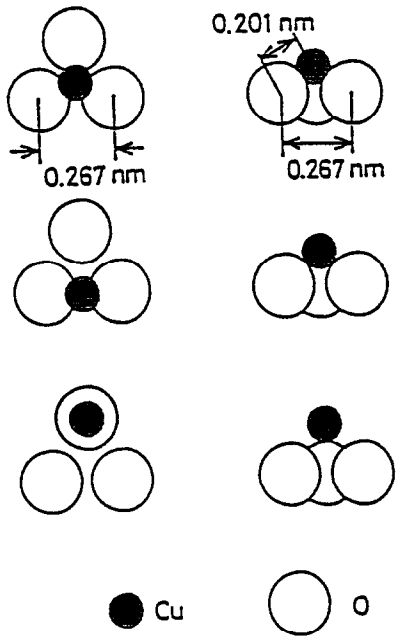

Fig. 7. Three possible sites for the location of Cu atoms on α-quartz (0001).

The Fourier transform of s- and p-polarized EXAFS spectra showed one peak between 0.1–0.2 nm which is straightforwardly assigned to Cu–O bond. The detailed analysis was conducted by a curve fitting method, demonstrating the existence of Cu–O bonds at 0.201 nm. No Cu–Cu bonding was observed in both s- and p-polarizations, indicating that Cu atoms were supported on α-quartz (0001) in a monomer form [15].

The N_i^*'s of Cu–O were determined to be 3.2 and 3.7 for s- and p-polarization, respectively, by the curve-fitting analysis ($N_p^*/N_s^* = 1.2$). There are three possible locations of Cu atoms on the α-quartz (0001); that is, 'atop', 'bridge', and 'three-fold hollow' sites as shown in Fig. 7. The N_i^*'s for these arrangements can be calculated by Eqs. (5–7). The electric-field vector is

$$N_i^*/3 = \cos^2\alpha \text{ (atop site)} \quad (5)$$

$$N_i^*/3 = 2\cos^2\alpha\cos^2\beta + 2\sin^2\alpha\sin^2\beta\cos^2\phi \text{ (bridge site)} \quad (6)$$

$$N_i^*/3 = 3\cos^2\alpha\cos^2\beta + 1.5\sin^2\alpha\sin^2\beta \text{ (three-fold hollow site)} \quad (7)$$

characterized by spherical coordinates α from the surface normal and ϕ in the surface plane, and β is the bond angle with the surface normal [23]. For the bridge sites, $\cos^2\phi$ was integrated in every direction because of equivalent positions. For the atop sites, only the EXAFS oscillation for the bonds normal to the surface can be observed, while there is no oscillation parallel to the surface.

Assuming the ideal surface structure with the O–O distance of 0.267 nm for the quartz [24] and using the Cu–O bond length (0.201 nm) determined by the EXAFS analysis, we found the agreement of the experimental results only with the Cu atoms being located on the three-fold hollow sites [15].

4.3. Cobalt oxides on α-Al_2O_3 (0001)

The samples were prepared by CVD using $Co_2(CO)_8$ as precursor which was deposited on α-Al_2O_3 (0001) for 2 h at room temperature, followed by evacuation at 313 K under vacuum to remove excess cobalt carbonyls (sample A). Then the sample (A) was exposed to O_2 at 300 K for 5 h and further oxidized in air at 873 K for 1 h to form the spinel-like sample (B) [19].

$$Co_2(CO)_8 + \alpha\text{-}Al_2O_3(0001) \rightarrow \underset{\text{(Sample A)}}{CoO_x/\alpha\text{-}Al_2O_3(0001)} \rightarrow \underset{\text{(Sample B)}}{[Co_3O_4]n/\alpha\text{-}Al_2O_3(0001)}$$

It was found that the sample (B) showed an extremely high activity for CO oxidation at 273 K as compared to a usual impregnation Co_3O_4/Al_2O_3 catalyst and to a Pt/Al_2O_3 catalyst [17,19]. The catalytic activity was so high that we could not follow the reaction rate. The sample (A) showed similar activity to that of the impregnation catalyst.

The arrangement of surface oxygen atoms on surface is hexagonal [24]. Similarly to the case of Cu ions on α-quartz (0001), assuming an ideal surface with O–O distance of 0.275 nm and using the Co–O bond length of 0.208 nm determined by the EXAFS analysis, we compared the observed ratio N_p^*/N_s^* to the calculated ones for the location models and concluded that Co atoms occupy the three-fold hollow sites far from Al atoms on the alumina. Such a selective adsorption may be due to a repulsive Coulomb interaction between Al atoms and Co atoms [19].

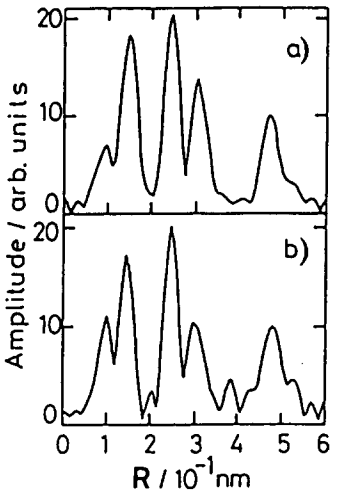

Fig. 8. Fourier transforms of polarized total-reflection fluorescence EXAFS for sample (B); (a) s-polarization and (b) p-polarization.

Oxidation of sample (A) at 873 K changed the EXAFS Fourier transform drastically, demonstrating the transformation of monomer structure to spinel structure in sample (B) as shown in Fig. 8. The Fourier transforms of the Co K-edge EXAFS data for the sample (B) in both polarizations in Fig. 8 resemble that for Co_3O_4 bulk spinel. The bond distances for 1st shell (Co–O), 2nd shell (Co(oct)–Co(oct)), 3rd shell (Co(oct)–Co(tet) + Co(tet)–Co(tet)), and 4th shell (Co(oct)–Co(oct)) were determined to be 0.193, 0.286, 0.341, and 0.496 nm, respectively, by a curve fitting analysis [17–19]. However, the N_i^*'s of the second and third peaks in Fig. 8 were different with s- and p-polarizations, suggesting asymmetric growth of spinel structure on α-Al_2O_3 (0001). Therefore, we tried the calculation of the ratio N_p^*/N_s^* in the second and third peaks for the several structural-model cases in which Co_3O_4 spinel (001), (110) and (111) planes grew parallel to the substrate (0001) plane. In each case, two kinds of layers are placed alternately. For the (001) plane, one layer consists of oxygen atoms and octahedral Co atoms (model-001A) and the

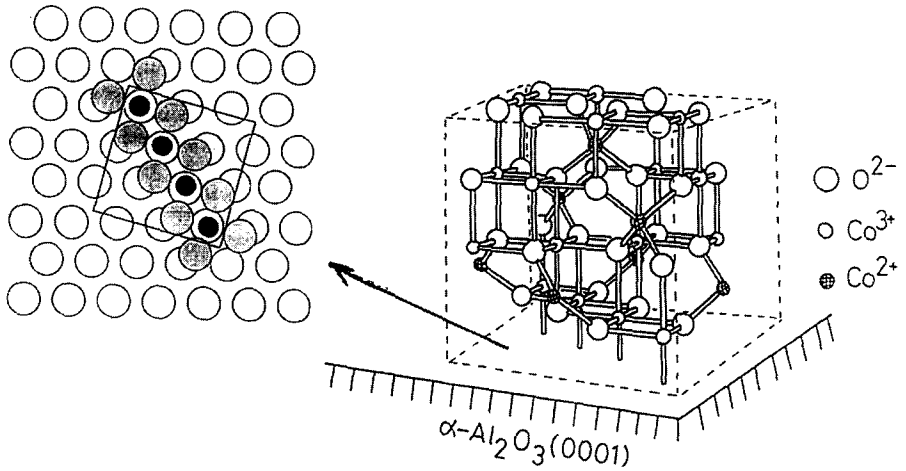

Fig. 9. Co_3O_4 spinel structure in 0.9 nm dimension with the (001) plane parallel to α-Al_2O_3 (0001) and an interface model (filled circles: Co atoms; shaded circles: O atoms of Co_3O_4 (001) plane; open circles: surface O atoms of α-Al_2O_3 (0001)).

other layer consists of tetrahedral Co atoms (model-001B). In case of the (110) plane, one layer consists of oxygen atoms and tetrahedral and octahedral Co atoms (110A), and the other layers consists of octahedral Co atoms and oxygen atoms (110B). For the (111) plane one layer is composed of oxygen atoms and octahedral Co atoms (111A), and the other layer is composed of tetrahedral Co atoms (111B). The expected ratios N_p^*/N_s^* were calculated for different layer numbers with these planes. It was found that the (001A) model with seven layers well reproduced the observed data for sample (B) [19]. No other models fit the observed ratio. The spinel structure of Co oxide with seven layers on α-Al_2O_3 (0001) is illustrated in Fig. 9.

The preferential growth of a close-packed (001) plane parallel to α-Al_2O_3 (0001) surface may be due to the repulsion between the surface oxygen atoms of α-Al_2O_3 (0001) and the interface oxygen atoms of Co_3O_4 (001) being less than the repulsion for other planes.

4.4. *Vanadium oxides on ZrO_2 (100)*

A Y_2O_3-stabilized ZrO_2 (100) was calcined at 673 K for 2 h in air to remove volatile residual. The ZrO_2 (100) plane is a stable surface and its top layer is composed of oxygen atoms [25]. $VO(OC_2H_5)_3$ was deposited on the ZrO_2 (100) by means of an impregnation method using an ethanol solution of $VO(OC_2H_5)_3$. The obtained samples were calcined at 823 K for 1 h in air. The 0.5 monolayer and 1.0 monolayer of vanadium oxide were supported on ZrO_2 (100) surface, where a monolayer is defined to be the amount of V atoms equal to the amount of surface oxygen atoms. The sample was put into the PTRF-XAFS chamber and fixed on the sample holder above described for observation in situ of the PTRF-XANES. Before the PTRF-XANES measurement, the sample was heated at 373 K for 1 h in situ in vacuum. To study the dissociative adsorption of V=O bonds with NH_3, NH_3 gas of 133 Pa was admitted to the sample at 423 K in the chamber.

The XANES spectra of one-monolayer vanadium oxides on ZrO_2 (100) surface are shown in Fig. 10(a and b). The pre-edge peak (1s→3d transition) was observed at 5467 eV for both spectra in s- and p-polarizations. The presence of the strong pre-edge peak in XANES suggests that vanadium atoms are located in a tetrahedral symmetry [26]. If the V_2O_5 (010) plane is exposed on ZrO_2 (100), the pre-edge peak intensity of the p-polarized XANES spectrum would show maximum and the intensity of the s-polarized one should show zero. In the XANES spectra of Fig. 10, the s-polarized pre-edge peak intensity was about half of the corresponding p-polarized

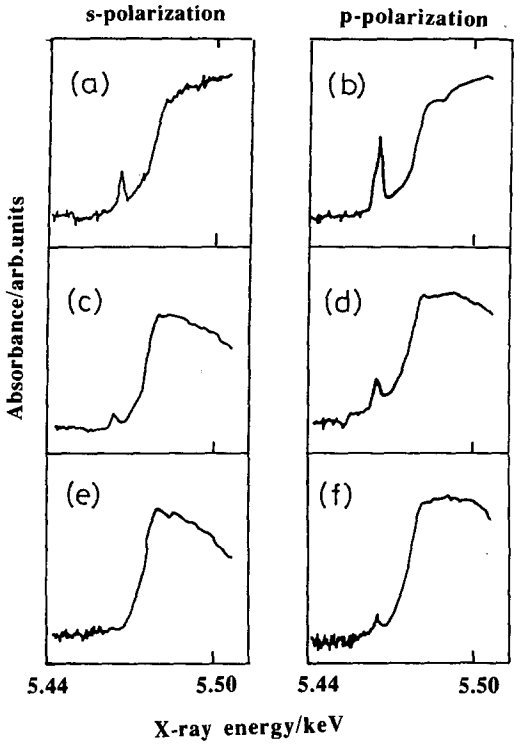

Fig. 10. In situ polarized total-reflection fluorescence XANES spectra of 1.0 monolayer vanadium oxide on ZrO_2 (100) in vacuum (a, b) and after NH_3 adsorption for 30 min at 423 K (c, d) and for 2 h at 423 K (e, f).

one. The angle between ZrO_2 (100) surface and V=O bond direction is not 90°. In the s-polarization spectra, the peak intensity should be integrated by the term $\cos^2\theta$ in every direction at the surface, where θ is the angle between the V=O bonds and the polarized direction of the incident X-ray in surface plane. It means that the peak intensity of the s-polarization spectrum is half the peak intensity of the p-polarization spectrum if the angle between the V=O bond and the polarization vector is the same in s- and p-polarization. This result may be explained by the arrangement of the V=O bonds of vanadium oxides which are inclined to the ZrO_2 (100) surface by about 45° [20]. The 45°-tilted V=O arrangement was observed with both the 0.5 and 1.0 monolayer vanadium oxides on ZrO_2 (100).

Upon NH_3 adsorption at 423 K, the pre-edge peak intensities of both s- and p-polarization spectra decreased in a similar way and became zero. The decrease of the pre-edge peak intensity is referred to the structural change from V=O to V–OH by the reaction with NH_3, where the vanadium oxide changes from tetrahedral structure to octahedral structure [20]. The similar decrease in the peak intensity of both polarizations may reflect a uniform orientation of the V=O bonds on ZrO_2 (100). All of the tilted V=O bonds on ZrO_2 (100) were active for the reaction with NH_3 at 423 K as shown in Fig. 10 [20].

References

[1] Y. Iwasawa, Catal. Today, 18 (1993) 21.
[2] Y. Iwasawa, Adv. Catal., 35 (1987).
[3] Y. Iwasawa, Tailored Metal Catalysts, Reidel, Dortrecht, 1986.
[4] J.C.J. Bart and G. Vlaic, Adv. Catal., 35 (1987) 1.
[5] D.C. Koningsberger and R. Prins (Eds.), X-ray Absorption Principles, Applications, Techniques of EXAFS and XANES, Wiley, New York, 1988.
[6] E.A. Stern, Phys. Rev., B10 (1974) 3027.
[7] B.K. Teo, EXAFS Spectroscopy: Basic Principles and Data Analysis, Inorganic Chemistry Concepts 9, Springer-Verlag, Berlin, 1986.
[8] J. Stohr, Ref. [5], p. 443.
[9] S.M. Heald, E. Keller and E.A. Stern, Phys. Lett., 103A (1984) 155.
[10] B. Lairson, T.N. Rhodin and W. Ho, Solid State Commun., 55 (1985) 925.
[11] L.R. Sharpe, W.R. Heinman and R.C. Elder, Chem. Rev., 90 (1990) 705.
[12] G. Martens, P. Rabe, N. Schwentner and A. Werner, Phys. Rev., B17 (1978) 1481.
[13] D.T. Jiang, N. Alberding, A.J. Seary and E.D. Crozier, Rev. Sci. Instrum., 59 (1988) 60.
[14] M.E. Herron, S.E. Doyle, K.J. Roberts, J. Robinson and F.C. Walsh, Rev. Sci. Instrum., 63 (1992) 950.
[15] M. Shirai, K. Asakura and Y. Iwasawa, Chem. Lett., (1992) 1037.
[16] M. Shirai, K. Asakura and Y. Iwasawa, Catal. Lett., 15 (1992) 247.
[17] K. Asakura, M. Shirai and Y. Iwasawa, Catal. Lett., 20 (1993) 117.
[18] M. Shirai, K. Asakura and Y. Iwasawa, Jpn. J. Appl. Phys., 32 (1993) 117.
[19] M. Shirai, T. Inoue, H. Onishi, K. Asakura and Y. Iwasawa, J. Catal., 145 (1994) 159.
[20] M. Shirai, K. Asakura and Y. Iwasawa, Catal. Lett., 26 (1994) 229.
[21] M. Shirai, M. Nomura, K. Askaura and Y. Iwasawa, to be published.
[22] K. Asakura, K. Tomishige, M. Shirai, W.-J. Chun, T. Yokoyama and Y. Iwasawa, to be published.
[23] J. Stohr, R. Jaeger and S. Brennan, Surf. Sci., 117 (1982) 503.
[24] R.W.G. Wrykoff, Crystal Structure, 2nd Ed., Interscience Publishers, New York, 1964.

25] M. Morinaga, M. Adachi and M. Tsukada, J. Phys. Chem. Solids, 44 (1983) 301.

[26] J. Wong, F.W. Lytle, R.P. Messmer and D.H. Maylotte, Phys. Rev., B30 (1984) 5596.